Biointerface Research in Applied Chemistry
Open-Access Journal (ISSN: 2069-5837)

Article
Volume 13, Issue 3, 2023, 262
https://doi.org/10.33263/BRIAC133.262

Effect of Sugarcane Juice Stabilized Synthesis of Hydroxyapatite Nanoparticles, Characterization and Morphology Studies

Rayal Balasundaram Thenmozhi [1], Raman Suresh [2], Balakrishnan Srividhya [3], Pitchaipillai Baskaran [4], Ramasamy Subramanian [1,*]

[1] PG & Research Department of Chemistry, Sun Arts and Science College, Tiruvannamalai-606755, Tamil Nadu, India; ksrcassubu@gmail.com (R.S);
[2] Department of Chemistry, Government Polytechnic College, Tiruvannamalai 606705, Tamil Nadu, India
[3] KSR College of Technology, Trichengode, Tamil Nadu 637 215, India
[4] Department of Physics, Government Arts College, Veppanthattai, Perambalur 621116, Tamil Nadu, India
* Corresponding author: ksrcassubu@gmail.com (R.S.);

Scopus Author ID: 15134457100
Received: 3.03.2022; Accepted: 29.04.2022; Published: 11.06.2022

Abstract: In the present work, synthesized sugarcane juice stabilized hydroxyapatite nanoparticles (HA NPs). The synthesis was carried out using different concentrations (5, 10, and 15 ml) of sugarcane juice. The HA-NPs were characterized by Fourier transform infrared (FTIR), X-ray diffraction (XRD), scanning electron microscope coupled with energy dispersive studies (SEM-EDAX). The morphology and elemental analysis were assessed by transmission electron microscope attached with selected area diffraction (TEM-SAED). The structure and morphology analysis of the synthesized HA-NPs indicate that the particles are crystalline in-phase and spherical. The morphology study of samples indicated that discrete and less agglomerated particles were produced at a high concentration (15 ml) of juice. This study reveals that sugarcane juice acts as a stabilizing agent as well as an organic modifier for the synthesis of HA-NPs.

Keywords: hydroxyapatite; sugarcane; stabilizing agent; morphology; organic modifier.

1. Introduction

Applications of nanomaterials are receiving more attention in the fields of biomedical optoelectronics, catalysis, and sensor devices, and in the field. The structure and morphology are significant in addition to the quantum size effects of the nanomaterials for their promising applications [1]. Calcium orthophosphate is the major constituent in biological systems due to calcium, which is a main component of the bone. HA-NPs play a key role in the fields of tissue engineering, dental implant coating, and orthopedic applications. The stoichiometric ratio of Ca and P in the ratio of 1:67corresponds to the human bone [2, 3]. The HA-NPs have outstanding biocompatibility and are widely used in bone tissue engineering and drug delivery systems [4]. It is well recognized that the structure and properties of HA-NPs are similar to those of bones and teeth. Consequently, HA-NPs are extensively used in orthopedic and dental applications for repairing the hard tissues and the drug delivery systems [5, 6]. The HA-NPs are readily biocompatible, making them easy to incorporate into inorganic materials to produce nanocomposites [7]. The HA-NPs have been synthesized by various methods such as spray pyrolysis [8], sol-gel method [9], solution combustion [10], hydrolysis [11], microwave [1],

solid-state reaction [12], hydrothermal reaction [13], mechano-chemical [14], and chemical precipitation method [15].

Among the synthesis methods, chemical precipitation is one of the common methods to produce HA-NPs for various applications. In addition to the chemical synthesis, the green synthesis of HA-NPs is of major interest among researchers due to their eco-friendly process. Especially, sugarcane juice influences the size, shape, and surface morphology of metal oxide nanoparticles, which are extremely useful in the evaluation of antibacterial activity [16, 17]. Many organic molecules and plant extracts have been used as stabilizing agents, capping agents, and surface modifiers to synthesize HA-NPs [18]. Plant extracts are the green substitute for traditional reagents used to inhibit the agglomeration of the particles during synthesis. Plant extracts are known to have various water-soluble phytochemicals that have reducing and antioxidant effects. Consequently, they are used to control the morphology and overcome the drawback of agglomeration during the synthesis of a wide range of nanoparticles [19].

Various plant extracts such as natural latex rubber, ginger root extract, *Tamarindus indica*, *Azadirachta indica* leaves, *Coccinia grandis* leaves, carrot peel, and rice seeds have been used as the green template for the synthesis of HA-NPs [20]. Green synthesis of HA-NPs has been successfully achieved using fruits such as mango, grapes, and ripe tamarind extracts [21]. Based on the literature survey, sugarcane juice has not been used as a stabilizing agent or surface modifier for synthesizing HA-NPs. It was aimed to use sugarcane juice as a green template to study the effect of size, shape, and morphology on the HA-NPs.

2. Materials and Methods

2.1. Reagents.

Calcium nitrate, diammonium hydrogen phosphate, and ammonium hydroxide were purchased from LobaChemie, Mumbai, India. Distilled water was used to prepare the solutions. Fresh sugarcane juice was received from the local vendor. The juice was centrifuged and filtered to remove solids and other impurities. The purified juice was used as a stabilizing agent for synthesizing hydroxyapatite nanoparticles.

2.2. Synthesis of hydroxyapatite.

Calcium nitrate (1.0 M) and diammonium hydrogen phosphate (DAHP) solution (0.6 M) were taken as precursors of Ca and P for the synthesis of HA-NPs by precipitation method [22]. The molar ratio of 1.67 was maintained during the synthesis. Briefly, 5, 10, and 15 ml of sugarcane juice were added to the calcium nitrate solution. Homogeneous mixing of the juice with calcium nitrate was confirmed. Afterward, 0.6 M of DAHP solution was added dropwise into the sugarcane juice-calcium nitrate mixture and constantly stirred for 4 h. The pH of the reaction mixture was maintained above 9 by adding ammonium hydroxide solution and then stirred for 12 h. As a result of stirring, the white precipitate obtained was thoroughly washed with distilled water. The precipitate was removed by centrifugation at 5000 rpm for 20 min.

Further, the precipitate was washed with acetone to remove organic impurities and then dried in a hot air oven at 110ºC for 4 h, crushed, and sintered at 500ºC for 3 h. The HA-NPs synthesized using 5, 10, and 15 ml of juice were named HA5, HA10, and HA15. A blank sample also synthesized with the same procedure without using sugarcane was named HA0.

2.3. Characterization methods.

Fourier transform infrared (FT-IR) spectrum was taken with a Jasco 6300 FT-IR spectrometer by the KBr technique. X-ray diffraction (XRD) was done using (Model: X'Pert-PRO) with Cu-Kα radiation at 30 kV. Diffraction angles scanned at 25 mA were 2θ- 80° at ambient temperature. The diffraction peak at 2θ=25.80°, matching (002) Miller's plane of HA-NPs, was chosen to calculate the crystallite size. Morphology, size, and shape were studied by scanning electron microscopy (JEOL Model JSM-6390LV). The SAED pattern is either a ring pattern or spots with variable orientation. The morphological feature was studied by the JEM JEOL-2100 transmission electron microscope (TEM). The elemental conformations were obtained by energy-dispersive X-ray spectroscopy (EDS).

3. Results and Discussion

3.1. Functional group analysis.

FT-IR spectroscopy analysis was carried out in the range of 400–4000 cm^{-1} to study the functional group transformation in sugarcane juice-stabilized HA-NPs, as shown in Figure 1. A broad peak at 3441 cm^{-1} was attributed to the absorbed moisture content in the samples. A narrow band at 565 cm^{-1} due to the OH^- deformation mode. The peak at 1637 cm^{-1} was attributed to the bending mode of water. The triply degenerate stretching bands at 1169, 1072, and 913 cm^{-1} are characteristic of P-O vibration. The bands noticed at 448, 500, and 521 cm^{-1} are due to the bending vibration mode of P-O of the (PO_4^{3-}) phosphate group [23].

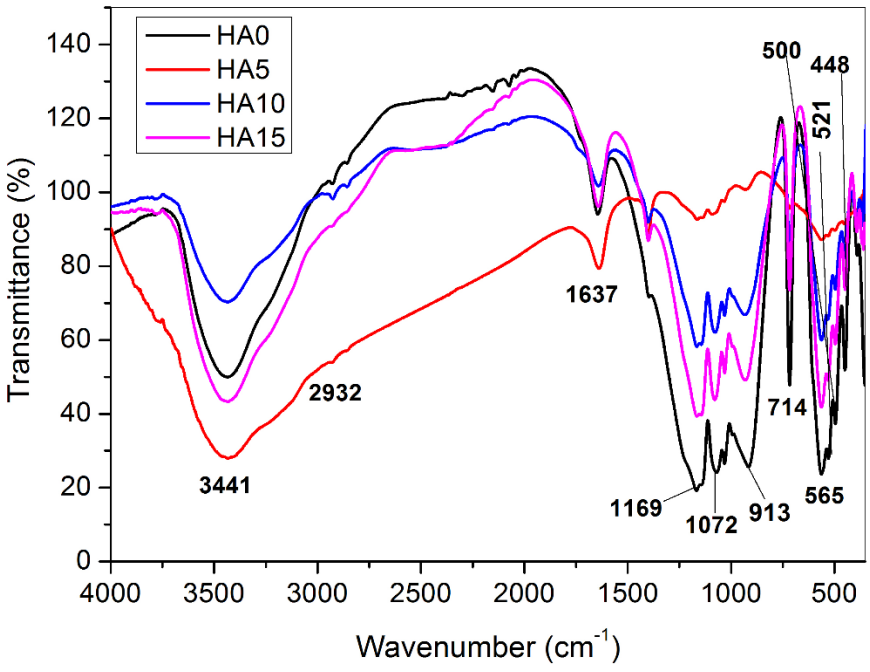

Figure 1. FTIR spectrum of hydroxyapatite; (HA0) HA-NPs without sugarcane juice; (HA5- HA15) HA-NPs with 5, 10, and 15 ml sugarcane juice.

3.2. Crystalline phase analysis.

TheXRDpattern of the HA-NPs synthesized with and without sugarcane juice is shown in Figure 2. Phase analysis was performed using PDF card no. 009-0432 for providing the information in the 2θ range of 10–80°. For HA-NPs produced with and without sugarcane juice, the diffraction pattern is in good agreement with the standard HA crystallites, which are well-

matched (JCPDS no. 009-0432). The corresponding planes were (002), (102), (210), (211), (202), (301), (310), (311), (312), (320), (004) and (420). This indicates that the synthesized nanoparticles are in hexagonal structures [24]. Extra peaks were observed due to a trace amount of calcium hydrophosphate. The sharp peaks observed in the XRD pattern of HA10 and HA15 synthesized in the presence of 10 and 15 ml juice reveal higher crystallinity. It was noticed that the increase in juice concentration promotes the growth of (102) and (301) planes [25]. The average crystallite of HA0, HA5, HA10, and HA15 was 24.27, 19.21, 15.38, and 13.85 nm, respectively.

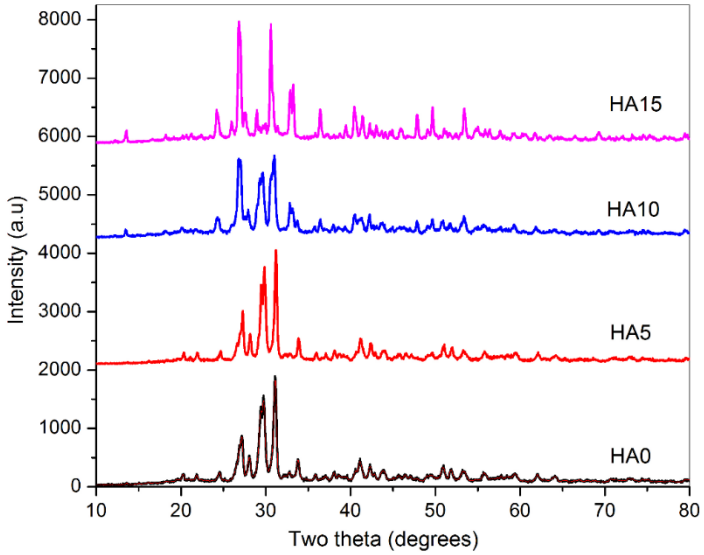

Figure 2. XRD spectra of hydroxyapatite; (HA0) HA-NPs without sugarcane juice; (HA5- HA15) HA-NPs with 5, 10, and 15 ml sugarcane juice.

3.3. SEM analysis.

The SEM images of the synthesized samples are shown in Figure 3 (HA0-HA15). HA0 represents the HA-NPs synthesized without sugarcane juice, exhibiting square-shaped nanoparticles. HA5 shows the SEM images of HA-NPs synthesized in the presence of 5 ml juice, which exhibits perfect square shape particles. When the juice volume was increased from 5 ml to 10 ml, irregular shape particles were observed, as shown in Figure 3 (HA10).

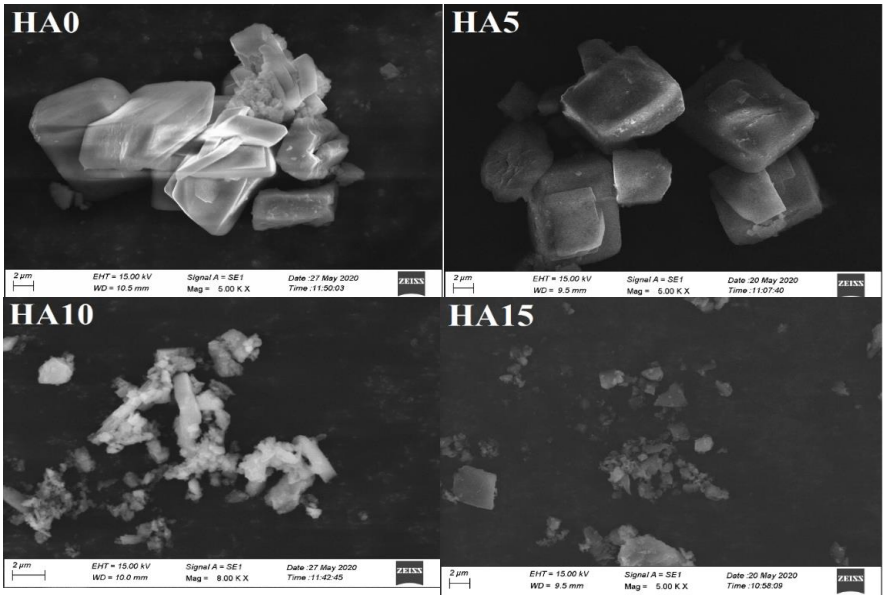

Figure 3. SEM images of HA synthesized without sugarcane juice (HA0) and with sugarcane juice (HA5-HA15) of 5, 10, and 15 ml sugarcane juice.

Visual inspection of the images indicates that the size of the particles observed in HA15 is smaller than those of the previous three samples (Figure 3 (HA15). Elemental compositions of HA0, HA5, HA10, and HA15 are shown in Figure 4. The EDS spectrum of each sample confirmed the presence of calcium, oxygen, and phosphorus.

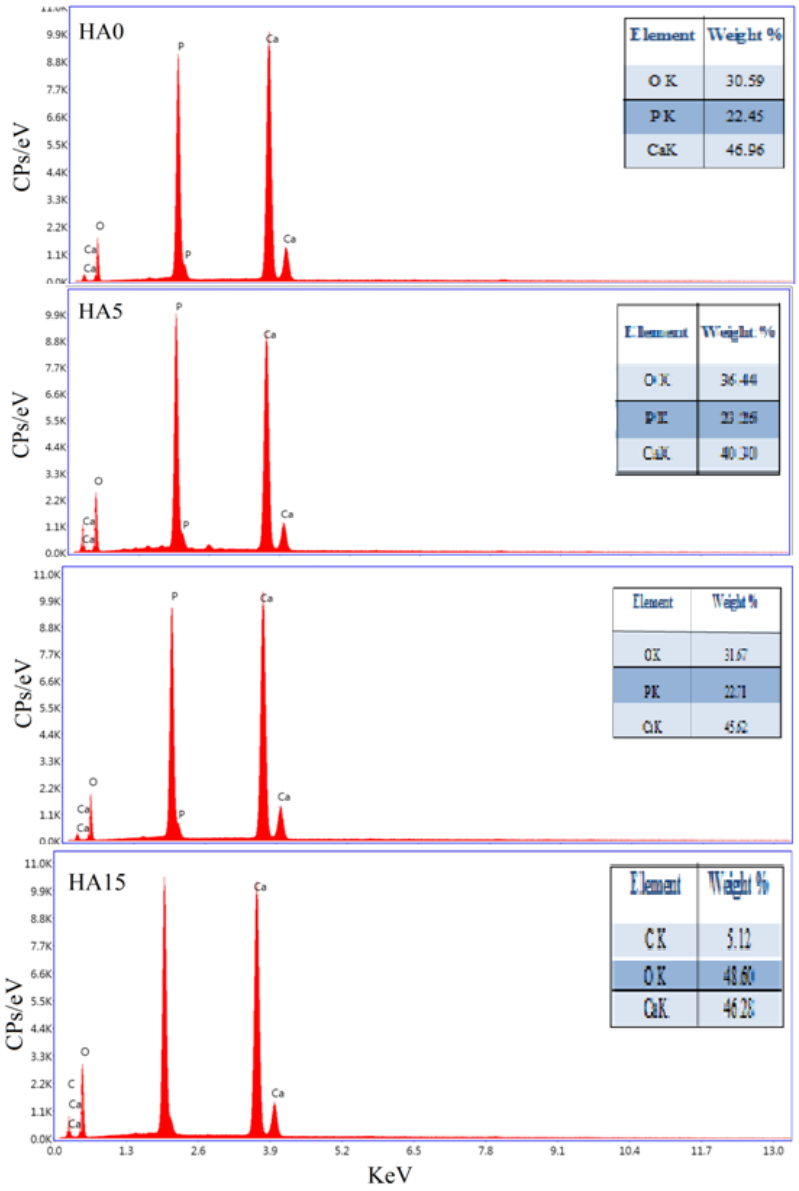

Figure 4. EDS spectrum of HA nanoparticles; (HA0) without juice (HA5-HA15) of 5, 10, and 15 ml sugarcane juice.

3.4. TEM morphology study.

The TEM morphology features of HA-NPs were analyzed using the TEM images (Figure 5(a-c)). The nanoparticles synthesized without juice show the existence of agglomerated particles (HA0). When the juice volume was 5 ml, the particles were found to be irregular and agglomerated. With the increase in juice concentration, the size of particles slightly increased with better dispersion. When the juice volume was 10 ml, the particles became spherical and well dispersed. The spherical particles continued to grow and became irregular when the juice volume was 15 ml (HA5). The reason is that sugarcane juice provides more nucleation sites at higher concentrations.

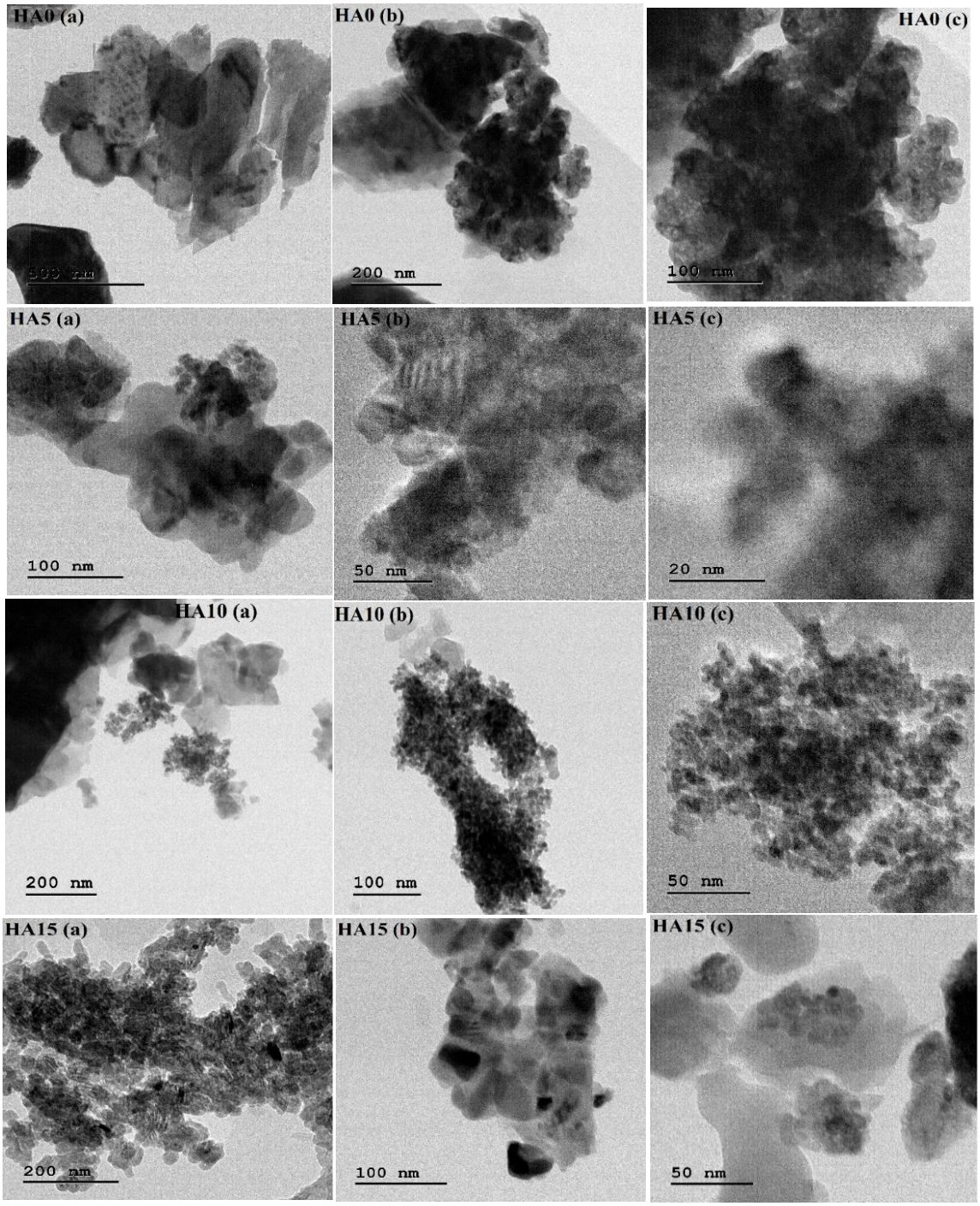

Figure 5. TEM images of hydroxyapatite; **(HA0)** without sugarcane juice; **(a-c)** TEM images taken at 200, 100, and 100 nm magnification; **(HA5)** with 5 ml sugarcane juice; (a-c) TEM images taken at 100, 50 and 20 nm magnification; **(HA10)** with 10 ml sugarcane juice, and **(HA15)** with 15 ml sugarcane juice: **(a-c)** TEM images recorded at 200, 100 and 50 nm magnification.

When the sugarcane juice concentration increased from 5, 10, and 15 ml, the shape of the particles transformed from irregular to spherical, the reason is that glucose, fructose, and other biomolecules present in the juice interact with the reaction mixture during the nucleation of particles, which leads to the formation of spherical-shaped particles. This indicates that the size and morphology of the nanoparticles can be controlled by adjusting the amount of sugarcane juice.

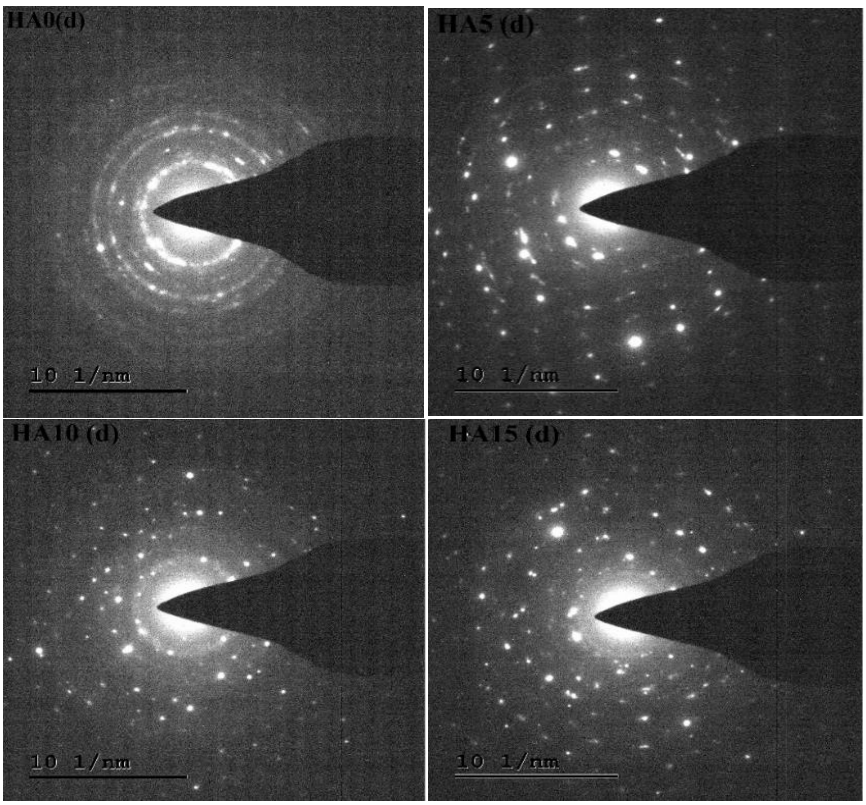

Figure 6. SAED pattern of HA nanoparticles; **(HA0)** without juice; **(HA5-HA15)** synthesized using 5, 10, and 15 ml sugarcane juice.

The size of the nanoparticles varies from 15 to 25 nm, according to TEM analysis. TheSAEDpattern of HA NPs is shown in Figure 6. The SAED pattern of all the HA0, HA5, HA10, and HA15 exhibits rings around the sharp spot, which displays the polycrystallinity of the samples. When sugarcane juice was used as a stabilizing agent, the formation of HA-NPs with smaller particles was due to the interaction between the OH andCOOHgroups and HA-NPs, which efficiently controlled the development of HA-NPs.

3.5. Formation mechanism of HA-NPs.

Sugarcane juice is a healthy and suitable drink with nutritional value. A tentative mechanism for synthesizing nanoparticles using sugarcane juice may be due to the presence of carbohydrates, which have functional groups such as carboxylic acid (COOH) and a hydroxyl group (OH). When the juice was added to the reaction mixture of calcium nitrate and ammonium phosphate, a calcium-hydroxyl/carboxyl complex was produced. Perhaps, electrostatic interaction between the carboxyl groups and Ca^{2+} ions present in the calcium nitrate takes place to produce a calcium-HA complex. Carbohydrate was eliminated from the calcium-juice complex during calcination at 500ºC. Therefore, through this mechanism, it can be concluded that sugarcane plays a reactive agent in the formation of nanoparticles.

Various plant extracts and biomaterials have been used as natural stabilizing agents to fabricate HA nanorods. *Moringa oleifera* flower extract has been used as a stabilizing agent to produce crystalline HA nanorods for bactericidal activity [1]. Gobi *et al*. have synthesized nano-HA using malic acid as a stabilizing agent and are recommended for biomedical applications [26]. Pectin isolated from the *Paprika biglobosa* has been used as a green template to produce HA-NPs. They reported nanoparticles from 17.5 to 26.3 nm [27].

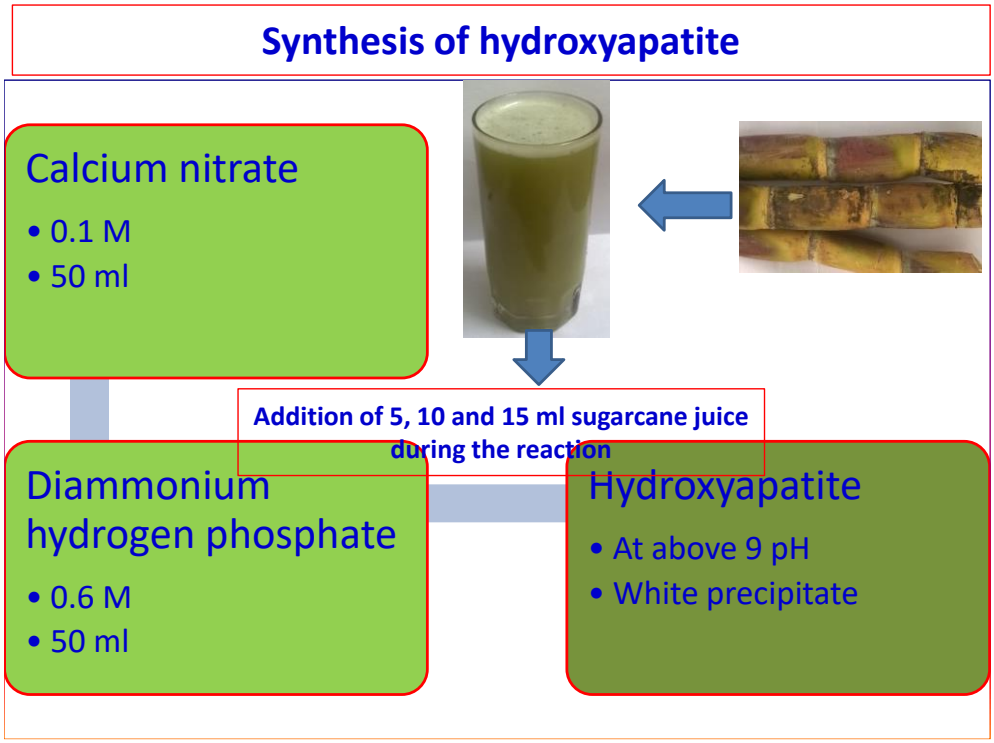

Figure 6. Mechanism and schematic diagram of the synthesis of hydroxyapatite nanoparticles

Anita Lett *et al*. Have synthesized mesoporous HA-NPs using stearic acid as an organic modifier by the sol-gel method and have suggested that it can be used for biomedical applications [28].

Table 1. Comparison of sugarcane juice with chemical stabilizers

S. No	Stabilizing agent	Effect of stabilizing agents	Ref.
1	EDTA	Chelating agents affect the morphology of HA and improve the crystallinity	[31]
2	Carboxymethyl cellulose (CMC)	HA-NPs using CMC as stabilizing agent	[32]
3	Citric acid or sodium citrate	Citric acid and sodium citrate addition improved the crystallinity and produced smaller sized HA-NPs	[33]
4	Tween-20	Influence the size and shape of the HA-NPs	[34]
5	Sulfonic acids and sulfonates	Influence the size and shape of the HA-NPs	[35]
6	Tween 20, trisodium citrate, and D-sorbitol	Influence the size and shape of the HA-NPs	[36]
7	Sugarcane juice	Influence the size and shape of the HA-NPs	[37]
8	Sugarcane juice	Stabilizing agent for silver nanoparticles	[38]
9	Sugarcane juice	Stabilizing agent for CuO NPs	[39]
10	Sugarcane juice	Stabilizing and capping agent for CuO NPs	[16]

Gum-acacia-assisted gold-HA-NPs with the range of 9-13 nm have been synthesized and explored its efficiency in the hydrogenation of nitrobenzene to aniline formation through gas-phase reaction [29]. Besides, the effects of metal oxide nanoparticles' size, shape, and morphology have been proved [30].

In addition, sugarcane juice has been used as stabilizing and capping agent for synthesizing metal and metal oxide nanoparticles (Table 1). Sugarcane juice is a very good source of carbohydrates. Carbohydrates present in the juice played a vital role as stabilizing

agents [40]. The effect of sugarcane juice on the size, shape, and morphology of silver nanoparticles, copper oxide nanoparticles, and hydroxyapatite nanoparticles has been reported.

4. Conclusions

Sugarcane juice stabilized synthesis of HA-NPs was carried out, and the structure of the HA-NPs was confirmed by using various spectral techniques. Among the synthesized samples (HA0, HA5, HA10, and HA15), no variations were found in the FT-IRanalysis. From the XRD pattern, the average size of the HA0, HA5, HA10, and HA15 was found to be 24, 19, 15, and 13, respectively. This confirms that there are size variations among the samples due to juice concentration. The SEM morphology of HA-NPs shows that at lower concentrations (5 ml), the particles were found to be spherical, whereas, at higher concentrations (15 ml), the particles became irregular in shape. Similarly, the TEM morphology results were similar to the SEM analysis. Both SEM and TEM morphology confirm sugarcane juice's role in forming particles.

Funding

This research received no funding from an external agency.

Acknowledgments

The authors thank The Director, Central Instrumentation Centre, St Joseph College, Trichy, for providing characterization facilities.

Conflicts of interest

The authors declare that there are no conflicts of interest.

References

1. Mondal, P.C.; Asthana, D.; Parashar, R.C.; Jadhav, S. Imprinting chirality in inorganic nanomaterials for optoelectronic and bio-applications: strategies, challenges, and opportunities. *Mater. Adv.* **2021**, *2*, 7620-7637, https://doi.org/10.1039/D1MA00846C.
2. AbouAitah, K.; Bil, M.; Pietrzykowska, E.; Szałaj, U.; Fudala, D.; Woźniak, B.; Nasiłowska, J.; Swiderska-Sroda, A.; Lojkowski, M.; Sokołowska, B.; Swieszkowski, W.; Lojkowski, W. Drug-Releasing Antibacterial Coating Made from Nano-Hydroxyapatite Using the Sonocoating Method. *Nanomaterials***2021**, *11*, 1690, https://doi.org/10.3390/nano11071690.
3. Grynyuk, I.I.; Vasyliuk, O. M.; Prylutska, S.V.; Strutynska, N.Y.; Livitska, O.V.; Slobodyanik, M.S. Influence of nanoscale-modified apatite-type calcium phosphates on the biofilm formation by pathogenic microorganisms. *Open Chem. J.* **2021**, *19*, 39–48, https://doi.org/10.1515/chem-2021-0199.
4. Liu, P.; Man, Y.; Bao, Y. Bioactive Porous Biocomposites Coated Magnesium Alloy Implant for Bone Rejuvenation Using a Fracture in Rat Model. *Biotechnol. Bioprocess Eng.* **2021**, *26*, 359–368,https://doi.org/10.1007/s12257-020-0006-9.
5. Rial, R.; González-Durruthy, M.; Liu, Z.; Ruso, J.M. Advanced Materials Based onNanosized Hydroxyapatite. *Molecules***2021**, *26*, 3190, https://doi.org/10.3390/molecules26113190.
6. Du, M.; Chen, J.; Liu, K.; Xing, H.; Songa, C. Recent advances in biomedical engineering of nano-hydroxyapatite including dentistry, cancer treatment and bone repair. *Compos. BEng.* **2021**, *215*, 108790, https://doi.org/10.1016/j.compositesb.2021.108790.
7. Mushtaq, A.; Zhao, R.; Luo, D.; Dempsey, E.; Wang, X.; Iqbal, M.Z.; Kong, X. Magnetic hydroxyapatite nanocomposites: The advances from synthesis to biomedical applications. *Mater. Des.* **2021**, *197*, 109269, https://doi.org/10.1016/j.matdes.2020.109269.

8. Fiume, E.; Magnaterra, G.; Rahdar, A.; Verné, E.; Baino, F. Hydroxyapatite for Biomedical Applications: A Short Overview. *Ceramics* **2021**, *4*, 542–563, https://doi.org/10.3390/ceramics4040039.
9. Kim, J., Kang, I.G., Cheon, K.H, Lee, S.; Park, S.; Hyoun-Ee Kim, H.E.; Han, C.M. Stable sol–gel hydroxyapatite coating on zirconia dental implant for improved osseointegration. *J. Materi. Sci. Mater. Med.* **2021**, *32*, 81, https://doi.org/10.1007/s10856-021-06550-6.
10. Obada, D.O.; Salami, K.A.; Oyedeji, A.N.; Fasanya, O.O.; Suleiman, M.U.; Ibisola, B.A.; Atta, A.Y.; Dodoo-Arhin, D.; Kuburi, L.S.; Dauda, M.; Dauda, E.T. Solution combustion synthesis of strontium-doped hydroxyapatite: Effect of sintering and low compaction pressure on the mechanical properties and physiological stability. *Mater. Lett.* **2021**, *304*, 130613, https://doi.org/10.1016/j.matlet.2021.130613.
11. Rial, R.; González-Durruthy, M.; Liu, Z.; Ruso, J.M. Advanced Materials Based onNanosized Hydroxyapatite. *Molecules* **2021**, *26*, 3190, https://doi.org/10.3390/molecules26113190.
12. Bulina, N.V.; Vinokurova, O.B.; Eremina, N.V. Prosanov, I.Y. Khusnutdinov, V.R.; Chaikina, M.V. Features of solid-phase mechanochemical synthesis of hydroxyapatite doped by copper and zinc ions. *J. Solid State Chem.* **2021**, *296*, 121973, https://doi.org/10.1016/j.jssc.2021.121973.
13. Ebrahimi, S.; Stephen Sipaut@Mohd Nasri, C.; Bin Arshad, S.E. Hydrothermal synthesis of hydroxyapatite powders using Response Surface Methodology (RSM). *PLoS ONE* **2021**, *16*, 0251009, https://doi.org/10.1371/journal.pone.0251009.
14. Xin, Y.; Shirai, T. Noble-metal-free hydroxyapatite activated by facile mechanochemical treatment towards highly-efcient catalytic oxidation of volatile organic compound. *Sci. Rep.* **2021**, *11*, 7512, https://doi.org/10.1038/s41598-021-86992-8.
15. Yang, X.; Guo, X.; Zhou, D.; Liu, J.K. High Anticorrosion Properties due to Electron Spin Polarization of Hydroxyapatite with Point Defects. *Ind. Eng. Chem. Res.* **2022**, *61*,4179–4190, https://doi.org/10.1021/acs.iecr.1c05023.
16. Angeline Mary, A.P.; Thaminum Ansari, A.; Subramanian, R. Sugarcane juice mediated synthesis of copper oxide nanoparticles, characterization and their antibacterial activity. *J. King Saud Uni. Sci.* **2019**, *31*, 1103–1114, https://doi.org/10.1016/j.jksus.2019.03.003.
17. Bhattacharjee, A.; Morya, V.; Ghoroi, C.; Enzyme-mimetic activity of sugar cane juice stabilized CuO nanospheres and CuO/GO nanocomposite: Green synthesis and applications. *Colloids Interface Sci. Commun.***2020**, *35*, 100239,https://doi.org/10.1016/j.colcom.2020.100239.
18. Singh, A.; Lal, U. R.; Mukhtar, H.M.; Singh, P.S.; Shah, G.; Dhawan, R.K. Phytochemical profile of sugarcane and its potential health aspects. *Pharmacog. Rev.* **2015**, *9*, 45–54, https://doi.org/10.4103/0973-7847.156340.
20. Martin, V.; Ribeiro, I.A.; Alves, M.M.; Gonçalves, L.; Claudio, R.A.; Grenho, L.; Fernandes, M.H.; Gomes, P.; Santos, C.F.; Bettencourt, A.F. Engineering a multifunctional 3D-printed PLA-collagen-minocycline-nanoHydroxyapatite scaffold with combined antimicrobial and osteogenic effects for bone regeneration. *Mater. Sci. Eng. C***2019**, *101*, 15–26, https://doi.org/10.1016/j.msec.2019.03.056.
20. Gopi, D.; Indira, J.; Nithiya, S.; Kavitha, L.; Kamatchi Mudali, U.; Kanimozhi, K. Influence of surfactant concentration on nanohydroxyapatite growth. *Bull. Mater. Sci.* **2013**, *36*, 799–805.
21. Buitrago-Vasquez, M.; Ossa-Orozco, C.P. Hydrothermal synthesis of hydroxyapatitenanorods using a fruit extract template. *Dyna (Medellin, Colombia)* **2018**, *204*, 283-288, https://doi.org/10.15446/dyna.v85n204.65773.
22. Subramanian, R.; Sathish, S.; Murugan, M.; Mohamed Musthafa, A.; Elango, M. Effect of piperine on size, shape and morphology of hydroxyapatite nanoparticles synthesized by the chemical precipitation method. *J. King Saud Uni. Sci.* **2019**, *31*, 667–673, https://doi.org/10.1016/j.jksus.2018.01.002.
23. Córdova-Udaeta, M.; Kim, Y.; Yasukawa, K.; Kato, Y.; Fujita, T.; Dodbiba, G.Study on the Synthesis of Hydroxyapatite under Highly Alkaline Conditions. *Ind. Eng. Chem. Res.* **2021**, *60*, 4385–4396, https://doi.org/10.1021/acs.iecr.0c05969.
24. Rodríguez-Lugo, V.; Karthik, T.V.K.; Mendoza-Anaya, D.; Rubio-Rosas, E.; Villaseñor Cerón, L.S.; Reyes-Valderrama, M.I.; Salinas-Rodríguez, E. Wet chemical synthesis of nanocrystalline hydroxyapatite flakes: effect of pH and sintering temperature on structural and morphological properties. *Royal Soc. Open Sci.* **2018**, *15*, 180962, https://doi.org/10.1098/rsos.180962.
25. Khan, F.S.A.; Mubarak, N.M.; Khalid, M.; Walvekar, R.; Abdullah, E.C.; Ahmad, A.; Karri, R.R.; Pakalapati,H. Functionalized multi-walled carbon nanotubes and hydroxyapatite nanorods reinforced with polypropylene for biomedical application. *Sci. Rep.* **2021**, *11*, 843, https://doi.org/10.1038/s41598-020-80767-3.

26. Arcos, D.; Vallet-Regí, M. Substituted hydroxyapatite coatings of bone implants. *J. Mater. Chem. B* **2020**, *8*, 1781-1800, https://doi.org/10.1039/C9TB02710F.
27. Ibraheem, S.A.; Audu, E. A.; Jaafar, M.; Adudu, J. A.; Barminas, J. T.; Ochigbo, V.; Igunnu, A.; Malomo, S.O. Novel pectin from *Parkia biglobosa* pulp mediated green route synthesis of hydroxyapatite nanoparticles. *Surf. Interfaces* **2019**, *17*, 100360, https://doi.org/10.1016/j.surfin.2019.100360.
28. Anita Lett, J.; Sundareswari, M.; Ravichandran, K.; Bavani Latha, M.; Sagadevan, S.; Bin Johand, M.R. Tailoring the morphological features of sol–gel synthesized mesoporous hydroxyapatite using fatty acids as an organic modifier. *RSC Adv.* **2019**, *9*, 6228, https://doi.org/10.1039/C9RA00051H.
29. Sreedhar, B.; Keerthi Devi, D.; Sai Neetha, A.; Pavan Kumar, V.; Chary, K.V.R. Green synthesis of gum-acacia assisted gold-hydroxyapatite nanostructures-Characterization and catalytic activity. *Mater. Chem. Phys.* **2015**, *153*, 23-31, https://doi.org/10.1016/j.matchemphys.2014.12.031.
30. Alves, J.O.; Tenório, J.A.S.; Zhuo, C.; Levendis, Y.A. Characterization of Nanomaterials Produced from Sugarcane Bagasse. *J. Mater. Res. Technol.* **2012**, *1*, 31-34, https://doi.org/10.1016/S2238-7854(12)70007-8.
31. Mishra, V.K.; Bhattacharjee, B.N.; Kumar, D.; Rai, S.B.; Parkash, O. Effect of chelating agent at different pH on spectroscopic and structural properties of microwave derived hydroxyapatite nanoparticles: A bone mimetic material. *New J. Chem.* **2016**, *40*, 5432-5441, https://doi.org/10.1039/C5NJ03322E.
32. Liu, R.; Lal, R. Effects of molecular weight and concentration of carboxymethyl cellulose on morphology of hydroxyapatite nanoparticles as prepared with one-step wet chemical method. *Front Environ. Sci. Eng.***2015**, *9*, 804–812, https://doi.org/10.1007/s11783-015-0785-y.
33. Li, C. Crystalline behaviors of hydroxyapatite in the neutralized reaction with different citrate additions. *Powder Technol.* **2009**, *192*, 1–5, https://doi.org/10.1016/j.powtec.2008.11.001.
34. Abdul Halim,.N.A., Hussein,M.Z., Kandar, M.K. Nanomaterials-Upconverted Hydroxyapatite for Bone Tissue Engineering and a Platform for Drug Delivery. *Int. J. Nanomed.* **2021,** 16, 6477-6496,https://doi.org/10.2147/IJN.S298936.
35. Miyazaki, T.; Imamura, M.; Ishida, E.; Ashizuka, M.; Ohtsuki, C. Apatite formation abilities and mechanical properties of hydroxyethylmethacrylate-based organic-inorganic hybrids incorporated with sulfonic groups and calcium ions. *J. Mater. Sci. Mater. Med.* **2009**, *20*, 157–161,https://doi.org/10.1007/s10856-008-3556-5.
36. Wang, A.; Yin, H.; Liu, D.; Wu, H.; Wada, Y.; Ren, M.; Xu, Y.; Jiang, T.; Cheng, X. Effects of organic modifiers on the size-controlled synthesis of hydroxyapatite nanorods. *Appl. Surf. Sci.* **2007**, *253*, 3311–3316, https://doi.org/10.1016/j.apsusc.2006.07.025.
37. Mitra, J.; Sharma, A. Luminescent, Ferromagnetic Silver Glyco nanoparticles: Synthesis to Annealing induced Substrate Specific Transformation. *RSC Adv.* **2015**, *5*, 28901-28907,https://doi.org/10.1039/C5RA01324K.
38. Mishra, A.; Sardar, M. Rapid biosynthesis of silver nanoparticles using sugarcane Bagasse—An Industrial Waste. *J. Nanoeng. Nanomanuf.* **2013**, *3*, 1–3, https://doi.org/10.1166/jnan.2013.1135.
39. Bhattacharjee, A.; Morya, V.; Ghoroi, C. Enzyme-mimetic activity of sugarcane juice stabilized CuO nanospheres and CuO/GO nanocomposite: Green synthesis and applications. *Colloids Interface Sci. Commun.* **2020**, *35*, 100239, https://doi.org/10.1016/j.colcom.2020.100239.
40. Khan, M.R.; Syed, A.; Zia, S.; Ahmed, W.; Aadil, R.M.; Manzoor, M.F.; Inam-Ur-Raheem, M.; Abid, M.; Shabbir, M.A.; Qureshi, S.; Din, A.; Karrar, E. Stabilization and attributive amelioration of sugarcane juice by naturally derived preservatives using *aonla* and *moringa extract*. *Food Sci. Nutr.* **2021**, *9*, 3048-3058, https://doi.org/10.1002/fsn3.2262.